Electronic Supplementary Material (ESI) for CrystEngComm.

Electronic Supplementary Information:

The Unexpected Discovery of the Ninth Polymorph of Tolfenamic Acid

Pietro Sacchi,[a] Susan M. Reutzel-Edens,[b,c] Aurora J. Cruz-Cabeza*[a]

[a] Department of Chemical Engineering and Analytical Science, University of Manchester, UK.
[b] Synthetic Molecule Design & Development, Eli Lilly and Company, Indianapolis, IN USA
[c] Cambridge Crystallographic Data Centre, 12 Union Road, Cambridge, UK CB2 1EZ

*Email: aurora.cruzcabeza@manchester.ac.uk

Table of contents

List of abbreviations
TFA – tolfenamic acid
XRD – X-ray diffraction
PXRD – powder X-ray diffraction
CSD – Cambridge Structural Database
CSS – Crystal Structure Similarity
PXS – Powder X-ray Similarity
TS – Tkatchenko-Scheffler dispersion correction
MBD – Many-body dispersion correction
ZPE – Zero Point Energy
FTIR – Fourier Transform Infrared Spectroscopy
CSP – Crystal Structure Prediction
IPA – isopropanol

S.1 Single crystal XRD data collection, solution and refinement

Table S1 shows the details for the data collection and the structure refinement. Data reduction has been performed with the *CrysalisPro* Software. Multi-scan absorption correction has been applied. Structure solution was performed with SHELXS, while the structural model was refined using SHELXL[1,2] using least-squares minimisation in Olex2.[3] Two samples from different batches were tested and preliminary data was indexed finding the same unit cell. Both crystal samples were weakly diffracting at higher theta angles and exposure times of 50s/frame were used for the data collection. Figure S1 shows the 50% ellipsoid plot for the TFA molecule in TFA-IX generated with Ortep3.[4] A complete list of bond lengths and angles is included in the Appendix. The geometrical parameters of the principal non-covalent interactions in the crystal structure of TFA-IX are reported in Table S2.

Table S1 details of the XRD data collection and refinement of TFA-IX

Data Collection	
Crystal size/mm^3	0.23 × 0.18 × 0.08
Reflections collected	16842
Unique reflections	3119
Reflections observed, $I > 4\sigma(I)$	1692
Completeness/%	91.1
R_{int}	0.0724
Refinement	
Max. resolution/Å	0.72
$R(F)$, $I > 2\sigma(I)$	0.0577
$wR(F^2)$, all	0.1247
Goodness-of-fit on F^2	1.038
Largest diff. peak/hole / e Å^{-3}	0.24/-0.24

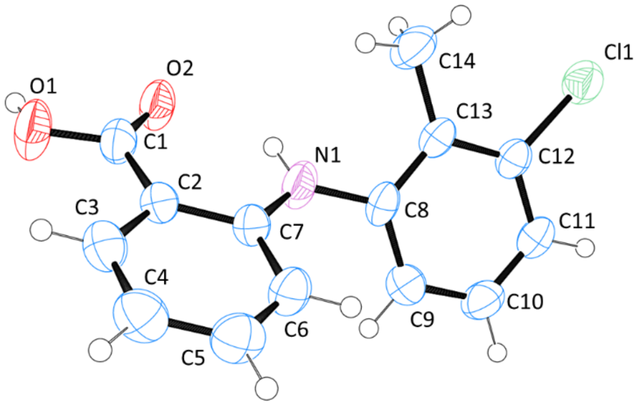

Figure S1 50% ellipsoid plot of the TFA molecule in TFA-IX

Table S2 Geometrical parameters of non-covalent interactions in the crystal structure of TFA-IX

Hydrogen Bonds						
Donor	**Acceptor**	**D-H (Å)**	**H...A (Å)**	**D...A (Å)**	**D-H...A (°)**	**Symmetry operation**
N1-H6	O2	0.84	1.990	2.684	139.1	x,y,z (intramolecular)
O1-H1	O2	0.84	1.825	2.666	175.9	1-x,-y,1-z
C14-H12	Cl1	0.96	2.824	3.736	158.7	-x,1/2+y,1/2-z

Other					
Type	**rings involved**	**$d_{centroid-centroid}$ (Å)**	**$d_{centroid-plane}$ (Å)**	**Angle (°)**	**Symmetry operation**
Aromatic stacking	$\mathrm{Ph_{Cl}}$-$\mathrm{Ph_{Cl}}$	3.794	3.426	25.4[a]	-x,-y,-z
T-type	$\mathrm{Ph_{COOH}}$-$\mathrm{Ph_{Cl}}$	2.874[b]	-	52.3[c]	x,1+y,z

[a] Angle between centroid-centroid and centroid-plane lines; [b] distance between the *para* H atom of the carboxylic acid ring and the centroid of the chlorine substituted ring; [c] Angle between planes containing the aromatic rings

S.2 Crystal form comparison

The crystal structure of TFA-IX was compared to the CSD crystal structures of TFA polymorphs to confirm that a new polymorph was found. Crystal structures were analysed visually and computationally with several methods. Fingerprint plots were generated from the Hirshfeld surfaces calculated using *CrystalExplorer*[5,6] and are shown in Figure S2 for TFA-I, TFA-II and TFA-IX.

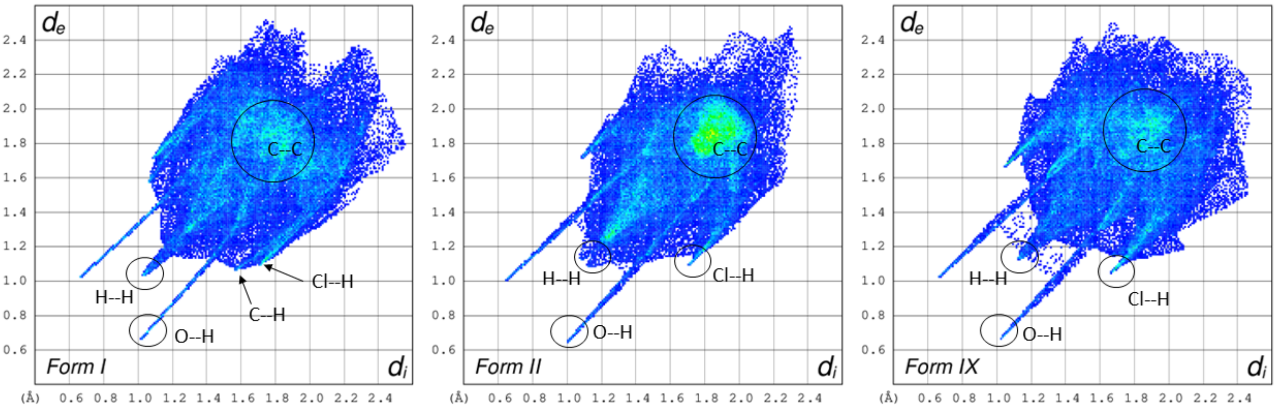

Figure S2 Hirshfeld surface fingerprint plots of the TFA molecules in TFA-I (left), TFA-II (middle) and TFA-IX (right). The atom--atom contacts which generate the relevant features are also shown.

The crystal structure of TFA-IX was compared to all of the CSD deposited structures of tolfenamic acid using the CSD Materials crystal packing similarity tool and the powder pattern similarity tool. Briefly, two powder patterns are considered the same if the PXS value is above 0.965.[7] The results of the comparison, namely the number of overlapping molecules (out of 20, 20% distance tolerance, 20° angle tolerance) with the associated rmsd and the powder pattern similarity are reported in Table S3 below.

Table S3 Numerical values of comparisons between crystal structures (CSS) and simulated powder patterns (PXS) of TFA-IX with structures of tolfenamic acid deposited in the CSD.

comparison				
Form	Refcode/s	CSS[a]	rmsd [Å]	PXS[b]
I	KAXXAI01/KAXXAI09	2	0.31	0.872
II	KAXXAI/KAXXAI10	2	0.79	0.933
III	KAXXAI02	5	0.35	0.945
IV	KAXXAI03	9	2.13	0.958
VI	KAXXAI08[c]	5	0.34	0.920
VII	KAXXAI05	5	0.31	0.925
VIII	KAXXAI06	2	0.75	0.912

[a]Crystal Structure Similarity (out of 20 molecules); [b]PXRD Similarity; [c]the other structure of TFA VI, KAXXAI07, is disordered. Comparison with Form V, KAXXAI04, was performed visually, as the disordered structure did not allow for automated comparison.

The simulated PXRD patterns of the TFA polymorphs are reported in Figure S3 below. We note a high similarity between the PXRD patterns of forms IV and VI (PXS value 0.986), between the PXRD patterns of form I and VIII (PXS value 0.980) and finally between the patterns of form III and IV (PXS value 0.977). We report in the main text that the DFT-optimised structures of forms IV and VI are identical (20/20 matching molecules and same energy minimum). The crystal packing similarity between the unoptimized structures is also high, with a value of 18 if a 20% tolerance on distances is used, which becomes 20 when the tolerance is increased to 50%.

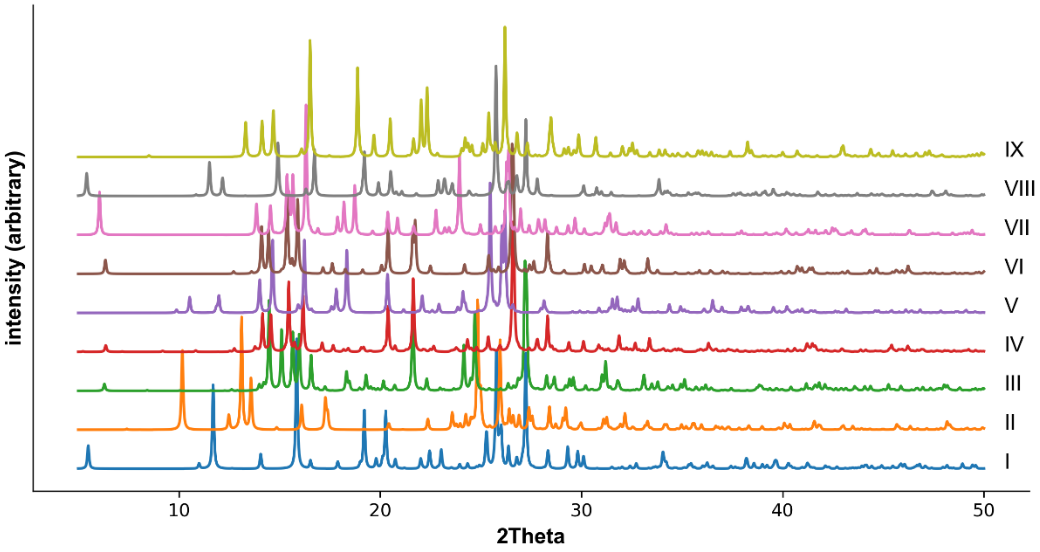

Figure S3 Simulated PXRD patterns of TFA polymorphs

S.3 DFT calculations

The experimental crystal structure of TFA-IX presented in this work was used as starting model for the DFT calculations. The structures of the remaining polymorphs were obtained from the CSD. For the disordered TFA-V (KAXXAI04), only the structure of the disorder component resulting most stable after the first optimisation step was used for further calculations; for TFA-VI, the ordered structure with refcode KAXXAI08 was used. The computed relative stabilities are compared with values from previous work in Table S4.

Table S4 Computed relative stabilities of TFA polymorphs at 0 K

			Periodic DFT-d (kJ/mol), PBE functional				
			Price et al.[8]		**This study**		
	CSD Refcode	**Packing coefficient (%)**	**TS**	**MDB**[a]	**TS**	**MBD**	**MBD+ZPE**
Form I	KAXXAI01	70.7	6.2	3.4	6.0	4.2	2.3
Form II	KAXXAI	71.8	0.0	0.0	0.0	0.0	0.0
Form III	KAXXAI02	70.4	9.0	6.9	7.8	5.3	4.4
Form IV[b]	KAXXAI03	70.6	8.3	-	7.6	5.1	4.5
Form V[c]	KAXXAI04	70.8/69.9	8.3/13.0	6.9	12.0	10.9	-
Form VI[b]	KAXXAI07 KAXXAI08	69.7	8.3/8.3	6.5/6.3	7.6	5.1	4.5
Form VII[c]	KAXXAI05	66.0	7.9	7.7	12.9	6.9	-
Form VIII	KAXXAI06	71.4	8.1	5.6	7.8	6.7	4.7
Form IX	This study	69.7	-	-	3.6	1.3	1.1

[a]Structures are geometry optimised at the PBE+TS level and a single point is then performed at the PBE+MDB level; [b]IV and VI optimise to the same structure; [c]vibrational modes were not calculated for V and VII

For the calculation of vibrational modes, supercells were built from the PBE-TS optimised structures. The dimensions of the supercells, together with the number of molecules in each cell, are reported in Table S5. When possible, supercells of at least 10x10x10 Å were used. The calculation for TFA-I required the use of a smaller supercell to reduce computational costs. The calculations for TFA-V and TFA-VII were unstable and it was impossible to eliminate imaginary frequencies despite several attempts with different calculation parameters. All of the other calculations resulted in no imaginary frequencies other than the three acoustic modes.

Table S5 Supercells used for vibrational analysis calculations

Form	Supercell	a	b	c	N$_{mol}$
I	3x1x1	14.075	32.175	8.035	12
II	3x1x1	11.230	21.895	14.278	12
III	2x1x1	15.2712	11.305	28.065	16
IV	2x1x1	15.2936	14.0179	18.273	12
V	2x2x2	15.3088	18.498	19.0848	12
VI	2x2x1	13.8714	14.603	14.0876	8
VII	2x1x2	13.496	29.153	14.2	16
VIII	2x1x3	16.005	16.4742	14.5266	12
IX	1x3x1	10.266	23.303	14.805	12

Figure S4 shows diagrams of thermodynamic quantities calculated from the phonon spectra of TFA polymorphs using the harmonic approximation. Our calculated values are compatible with the ranges reported for similar calculations.[9] The entropic contribution in TFA-I is almost always the smallest (thus lower relative free energy) in each of the considered pairs of polymorphs.

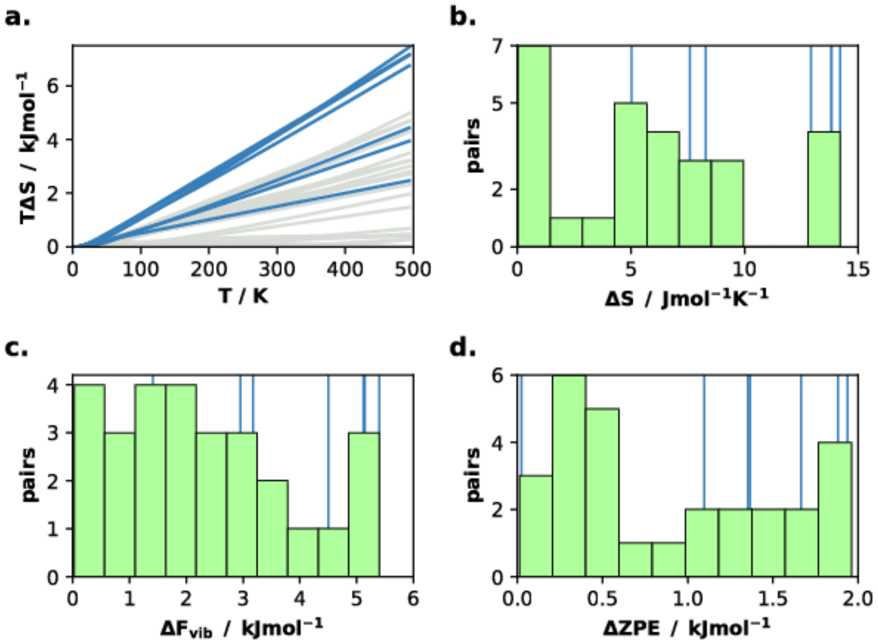

Figure S4 Difference in entropic contributions to free energies between pairs of TFA polymorphs with blue lines indicating when TFA-I is in the pair (a) and distributions of differences in entropy at 300 K (b), differences in vibrational energies at 300 K (c) and differences in zero-point energies (d) between pairs of TFA polymorphs. The blue vertical lines indicate when TFA-I is in the pair.

As discussed in the main text, the calculation of vibrational contributions to the lattice energies can strongly improve the relative energy ranking of polymorphs. We note, however, that the computational costs of this method remain high. Each calculation of the lattice phonon modes took on average 76 hours running on 96 cores (2.6 GHz). A systematic reduction of a CSP landscape with hundreds of predicted structures using this method would require immense computational time, and other computational strategies may be preferable for this task.[10]

S.4 Vibrational frequencies analysis

In spite of their high computational cost, our DFT calculations of vibrational frequencies greatly improve the estimation of the relative stability of the TFA polymorphs, and their performance is reflected in the remarkable similarity between the ZPE energy differences and the measured DSC enthalpy differences between the three forms I, II and IX (see Table 2 in the main text). In order to evaluate the possible origin for the calculated differences in ZPE, we have analysed more in detail the vibrational modes of the TFA polymorphs, with a focus on the three main polymorphs presented in this paper (I,II and IX) and their molecular conformation.

We collected FTIR spectra of TFA-I and TFA-IX powders using a Thermo Scientific Nicolet iS10 Spectrometer equipped with a Smart iTR Attenuated Total Reflectance Sampling Accessory in the 4000-600 cm^{-1} range. The measured frequencies for the N-H stretch and for the C=O stretch peaks are compared in Table S6 with data published for TFA-I and TFA-II by Wittering et al.[11]

Table S6 frequencies of the N-H and C=O stretch peak from FTIR data for TFA-I and TFA-IX

Frequency (cm^{-1})		TFA-I	TFA-II	TFA-IX
N-H stretch	Wittering et al.	3339	3322	-
	This work	3338.8	-	3334.9
C=O stretch	Wittering et al.	1654	1659	-
	This work	1654.7	-	1647.0

The collected FTIR spectra of TFA-I and TFA-IX are shown in Figure S5. The two spectra look very similar, especially at higher frequencies, while some differences in the peak shapes in the 1800-600 cm^{-1} region are more evident. This is not surprising, considering that the TFA molecules in the crystal structures interact with the same carboxylic acid hydrogen bond motif, and that differences in crystal packing arise from secondary aromatic interactions.

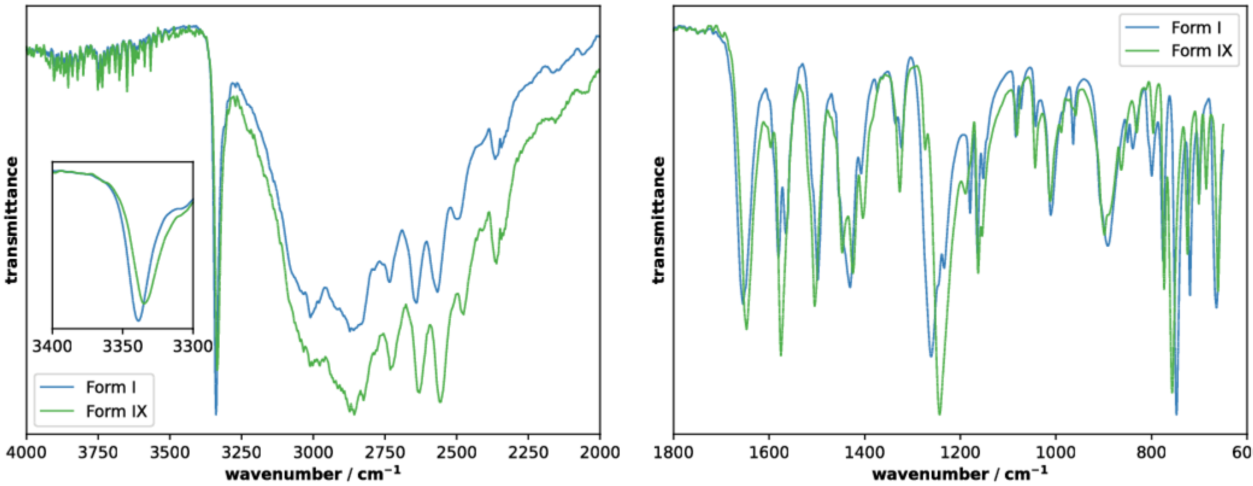

Figure S5 FTIR spectra of TFA-I (blue line) and TFA-IX (green line) powders in the 4000-2000 cm^{-1} range (left) and in the 1800-600 cm^{-1} range (right). The inset shows a detail of the peaks corresponding to the N-H stretch. The transmittance was normalised in both spectra to simplify their visualisation.

The high-frequency modes of TFA-I have slightly higher frequencies than TFA-II and TFA-IX both in the measured FTIR data and in the calculated DFT results. However, in the lower frequency range, the frequencies of TFA-II and TFA-IX are larger (Figure S6) and they have a more profound effect on the total calculated ZPE. To show this, we have calculated the contribution of phonon modes belonging to three different frequency intervals on the total ZPE, and the results are presented in Table S7.

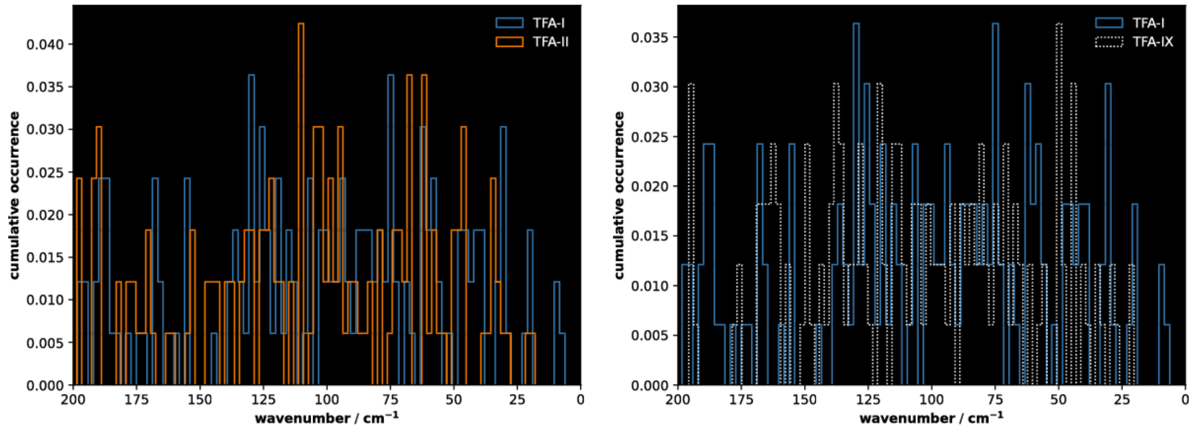

Figure S6 Histograms of lattice vibrational modes calculated with DFT for TFA-I (blue lines), TFA-II (orange lines) and TFA-IX (white dotted lines).

Table S7 Contributions to the total ZPE arising from the vibrational modes in TFA polymorphs. All energies are relative to the smallest value for each set. The percentage values in parentheses indicate the fraction of vibrational modes falling in the selected range.

		ΔZPE (kJmol^{-1})	High (13 %)	Mid (72 %)	Low (15 %)
form	conformer	total	3500 - 2500 cm^{-1}	2500 – 200 cm^{-1}	200-0 cm^{-1}
I	T	0.0	0.3	0.0	0.0
II	P	1.9	0.0	1.8	0.4
IX	P	1.7	0.0	1.4	0.5
III	P	1.1	0.0	1.6	0.2
IV	P	1.4	0.1	1.4	0.6
VI	P	1.4	0.0	1.4	0.6
VIII	T	0.0	0.6	0.0	0.1

In the high-frequency range, the contribution to the total ZPE is higher for TFA-I and TFA-VIII. The contribution to the total ZPE from the mid and low frequency modes, however, is the smallest for these two structures, and this results in their total ZPE contribution being the smallest in all the TFA polymorphs. The contribution of the mid-frequency range modes is the highest overall, although this is likely due to the large interval of frequencies considered for their calculation. Overall, these results suggest that the low frequency modes, and the lattice vibrational modes in particular, have a greater impact on the calculated differences in ZPEs.

S.5 TFA-IX crystals – morphology and crystallisation

The experimental morphology of TFA-IX crystals indexed using the *CrysalisPro* Software is shown in Figure S7. Manual measurements of relevant interfacial angles were performed on microscope images of several crystals and were consistent with the indexed morphology.

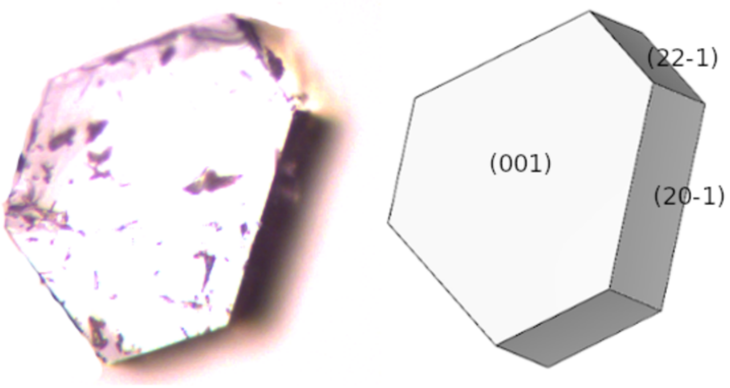

Figure S7 Single crystal of TFA-IX used for XRD data collection (left) and related crystal shape with facets indexed from XRD data (right).

As described in the main text, smaller crystals (about 0.2 mm) appeared colourless, while bigger crystals (over 1 mm) were of a clear, pale yellow colour. Crystals obtained from the procedure described in the Methods section were manually isolated from concomitant crystals of TFA-I and TFA-II and used as seeds for growth in IPA solutions. The grown seeds (Figure S8) were ground to powders which were analysed with PXRD to confirm phase identity.

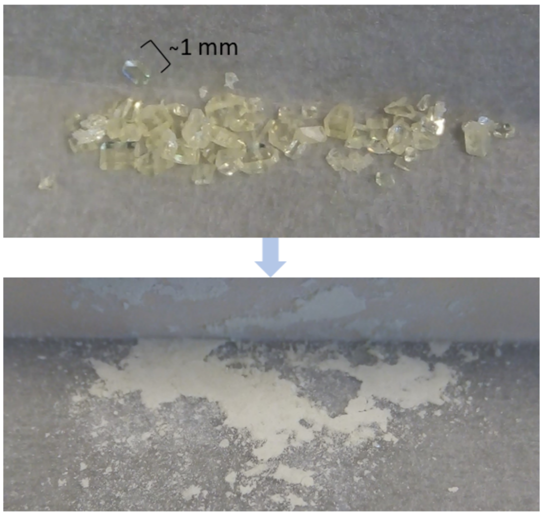

Figure S8 Pale-yellow crystals of TFA-IX grown from IPA solutions (top) were crushed into powders for further use (bottom).

The pure powders were then used for seeded batch crystallisations in IPA solutions starting at around 25 °C and decreasing the temperature to 19 °C over the course of several hours. Indicatively, 10 mg of initial seeds resulted in about 100 mg of product. The resulting powders were analysed with PXRD and used for thermal analysis, solubility measurements and slurry experiments.

S.6 Thermal analysis of TFA-II and TFA-IX transformation

The solid state phase transformation of TFA-II to TFA-I had been reported in previous works and the measured DSC values are summarised in Table S8.

Table S8 Summary of DSC measured values for the TFA-II to TFA-I transformation

	T_{onset} (°C)	T_{onset} (K)	ΔH_{trans} (kJ/mol)
Mattei et al.[12]	141.8	414.9	1.1
Du et al.[13]	157	430	0.7
This work	144.2	417.3	1.41

In the case of TFA-IX, a small endothermic peak at 135 °C was observed. We verified that this peak corresponds to the solid-solid transformation to TFA-I. The transformation takes place quickly, with the formation of a multitude of needle crystals and loss of crystallinity (Figure S9).

Figure S9 Hot stage microscopy images of a single crystal of TFA-IX before (left), during (middle) and after (right) the transformation to TFA-I. The temperature in Celsius degrees is shown in the bottom right corner. The Hot-stage experiment was performed using silicon oil to avoid sublimation and growth of TFA-I.

A few big crystals (pale-yellow) of TFA-IX were heated to about 160°C and PXRD data was collected on the resulting white polycrystalline sample. Figure S10 shows the measured powder pattern compared to data collected for a pure sample of commercial TFA-I.

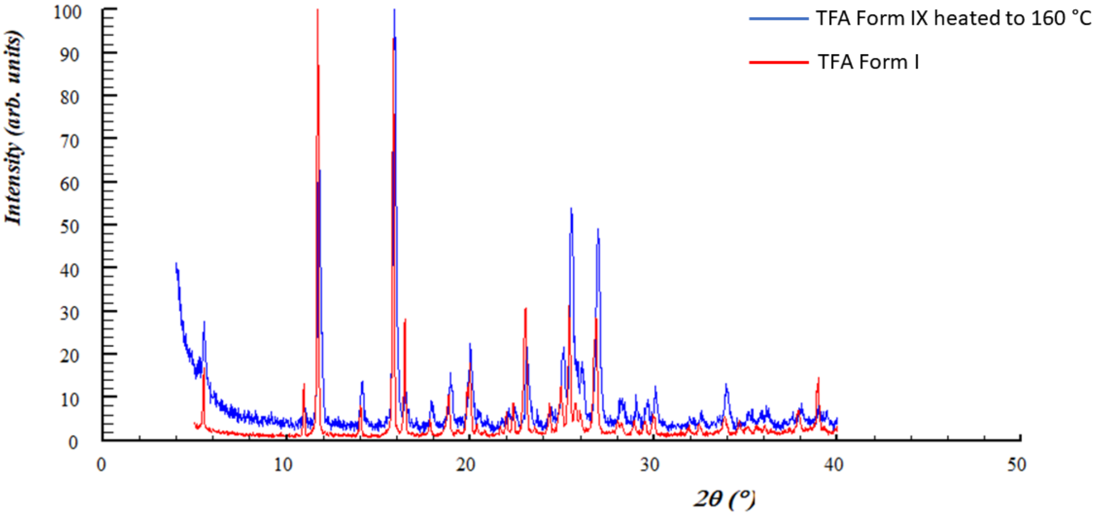

Figure S10 Experimental PXRD patterns of TFA-IX crystals heated to 160°C (blue line) and commercial TFA-I (red line).

The effect of the heating rate of the DSC measurements on the TFA-II and TFA-IX samples were also tested. Faster heating rates resulted in shifting the onset of the endothermic peak of the solid-solid phase transitions to higher temperatures, while the onset temperature of the melting peak of TFA-I was not affected (Figure S11). Figure S12 shows this effect on the transformation of TFA-II to TFA-I for five different heating rates up to 80Kmin^{-1}. Due to scarce sample availability, this curve was not constructed for TFA-IX.

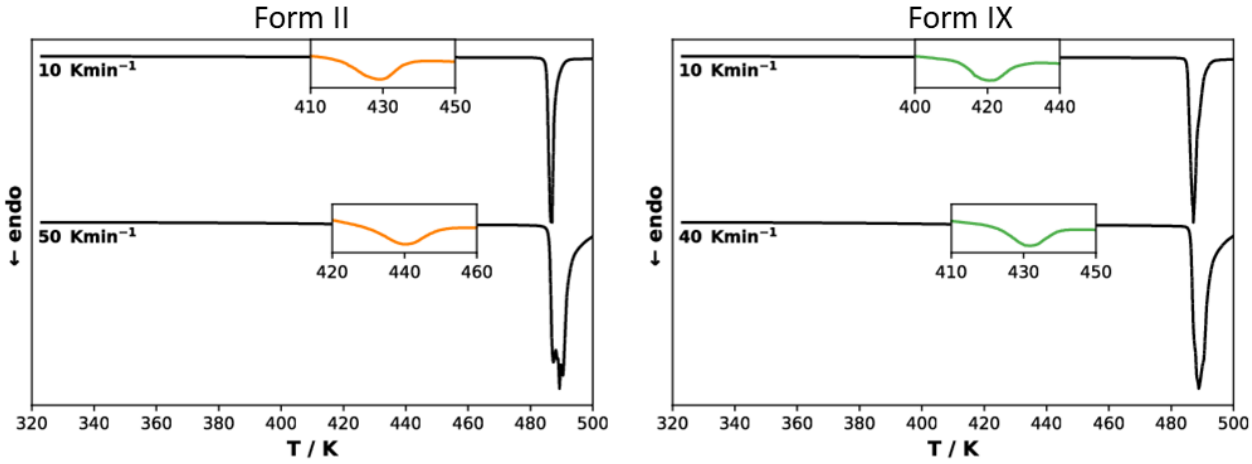

Figure S11 DSC curves of TFA-II (left) and TFA-IX (right) measured using different heating rates.

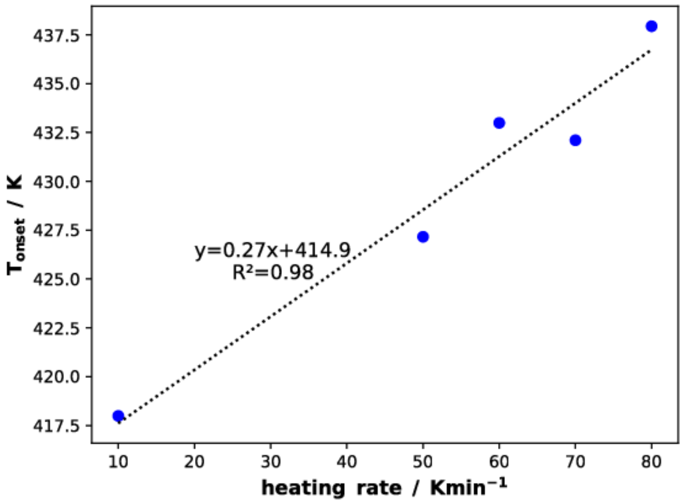

Figure S12 Effect of different heating rates on the onset temperature of the endothermic transformation of TFA-II to TFA-I.

S.7 Slurry experiments

The stability of TFA-IX was verified experimentally by slurry experiments with the procedure described in the main text. Experiments resulted in the transformation of TFA-IX to the more stable TFA-II (Figure S13). At 40°C TFA-I nucleated after about 10 minutes.

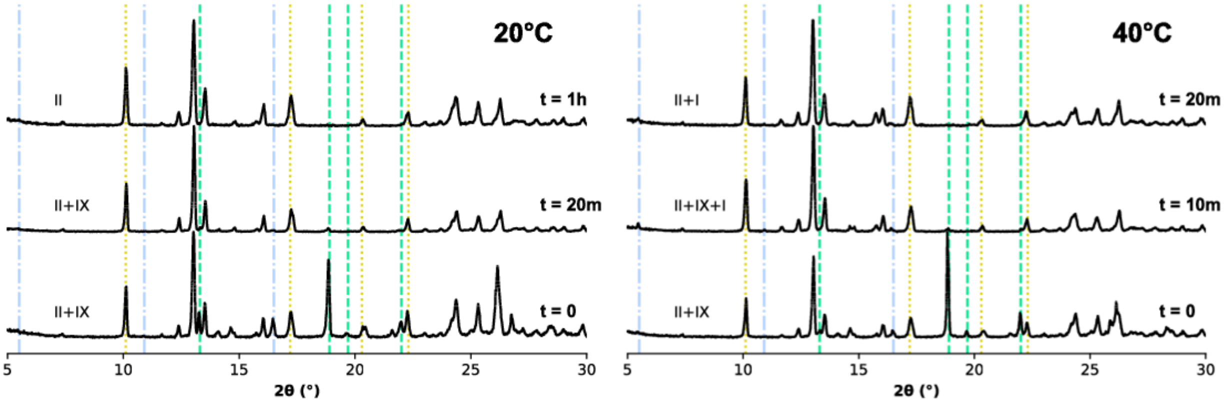

Figure S13 Normalised PXRD patterns of the excess solids at three different time intervals of the slurry experiments in IPA at 20°C (left) and 40°C (right) initiated from a 50%:50% IX:II mixture. A number of representative diffraction peaks for each form were drawn to aid phase identification: form I (blue, dash-dotted line), II (orange, dotted line) and IX (green, dashed line).

S.8 Solubility measurements

Table S9 reports the measured values in molar fraction for the solubilities of TFA-I,TFA-II and TFA-IX in IPA at various temperatures, as obtained using the turbidimetry procedure described in the main text. Our measured values for TFA-I and TFA-II are compared with previously published data[13] in Figure S14. Molar fraction solubilities were calculated as:

$$x = \frac{mol_{solute}}{mol_{solute} + mol_{solvent}}$$

The temperature reported in the table is modified according to calibration experiments performed on the Crystal16 to ensure a correct correspondence between the actual temperature in the sample vials and the temperature read from the equipment's software.

Table S9 Molar fraction solubilities of TFA polymorphs in IPA measured in this work

TFA-I				TFA-II				TFA-IX		
T (K)	x	σ_x[a]		T (K)	x	σ_x		T (K)	x	σ_x
286.6	0.00331	3e-05		291.1	0.00309	3e-05		290.1	0.00325	3e-05
294.3	0.00412	3e-05		291.6	0.00334	3e-05		292.8	0.00368	3e-05
300.9	0.00481	3e-05		293.0	0.00276	3e-05		296.6	0.00466	3e-05
307.8	0.00586	3e-05		296.7	0.00406	3e-05		302.9	0.00433	3e-05
310.5	0.00694	3e-05		299.0	0.00385	3e-05		308.6	0.00604	3e-05
312.4	0.00694	3e-05		302.2	0.00495	3e-05		316.1	0.00533	3e-05
312.4	0.00694	3e-05		303.3	0.00529	3e-05				
317.1	0.00857	3e-05		305.7	0.00509	3e-05				
317.6	0.00857	3e-05		308.3	0.00639	3e-05				
317.1	0.00857	3e-05		313.4	0.00792	3e-05				
320.6	0.00941	3e-05								
[a] the error is propagated from the error on the measurement of the solute and solvent sample masses (1e-4 g)										

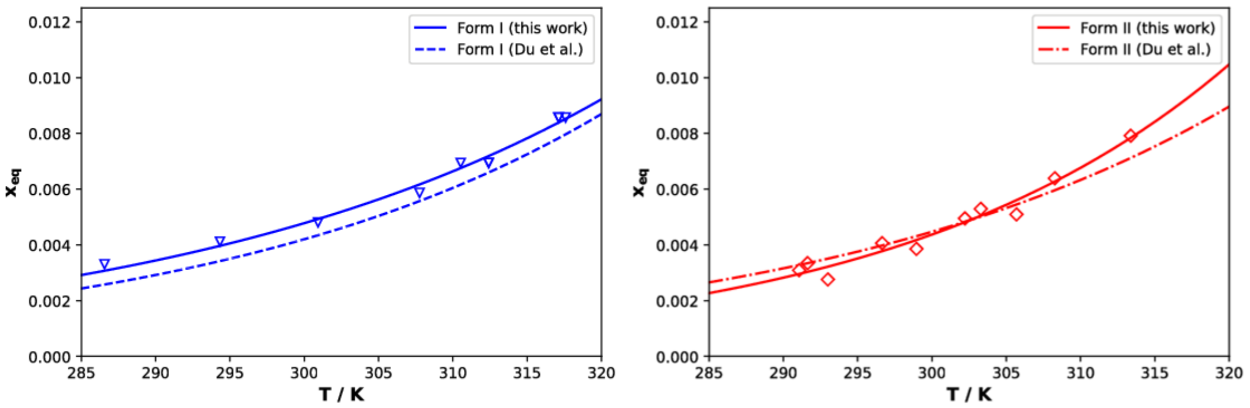

Figure S14 Solubility curves of TFA-I (left, blue triangles) and TFA-II (right, red diamonds) measured in this work and their exponential fits (solid lines) are compared to data published by Du and co-workers (exp. fit, dashed lines).

S.9 Patent CN107814733A

The new polymorph of TFA presented in this work was reported in a recent patent document.[14] The crystal form is identified in the patent by images of a PXRD pattern, a DSC curve and an infrared spectrum. The former was compared visually with a PXRD pattern simulated from the crystal structure of TFA-IX (Figure S15) and with an experimental FTIR spectrum (Figure S16). The resemblance between the two patterns suggests that the crystal form F presented in the patent and TFA-IX are the same polymorph. We note, however, that any attempt of reproducing the crystallisation procedures described in the patent failed to yield the desired form IX and resulted instead in the crystallisation of the known TFA-I and TFA-II.

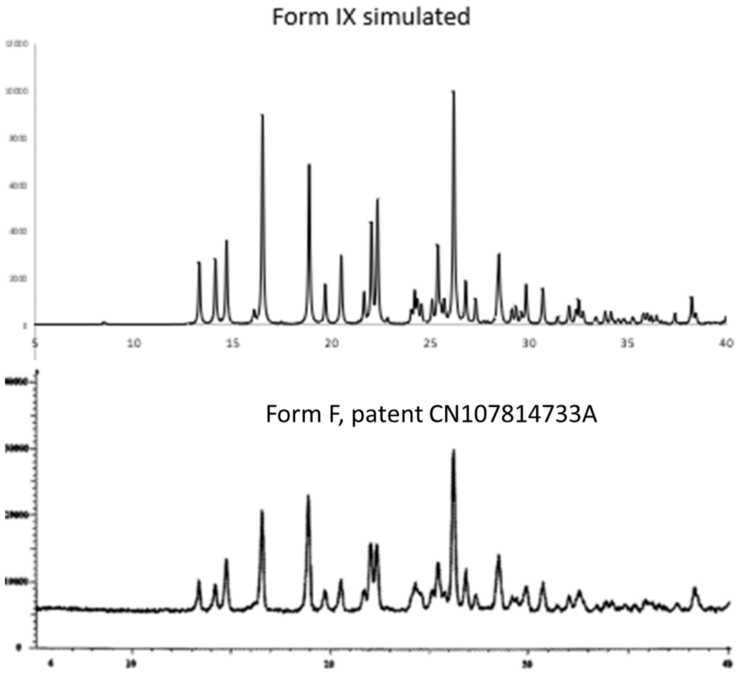

Figure S15 Simulated PXRD pattern of TFA-IX (top) compared to the pattern of Form F (bottom), as published in patent CN107814733A

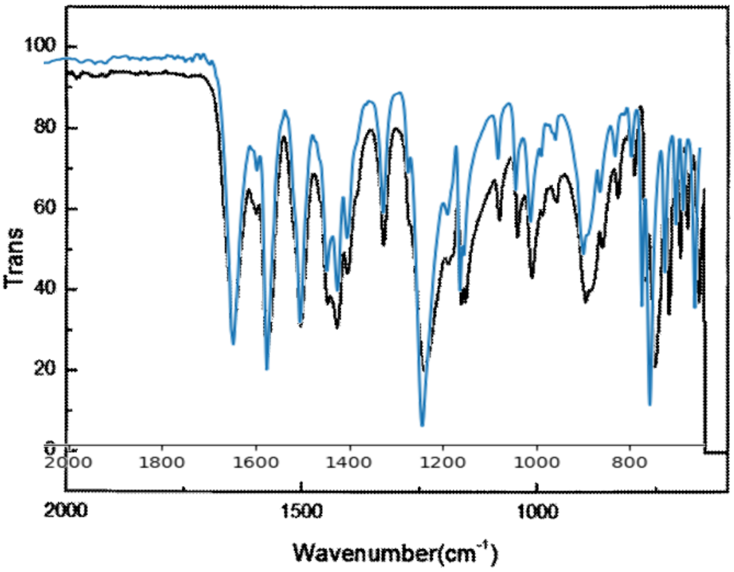

Figure S16 Overlay of the experimental FTIR spectrum of TFA-IX (blue) with the FTIR spectrum of Form F (black) as published in patent CN107814733A

S.10 Dimer interaction energies

Intermolecular interaction energies were calculated for pairs of molecules extracted from DFT optimised structures applying the MBD dispersion correction. The relevant interaction geometries were first identified by visual observation of the crystal structures and with the use of UNI intermolecular potentials as implemented in CSD Mercury.[15,16] Extracted dimers (excluding hydrogen-bonded pairs) and monomers were then placed in a simulation cell of 30x30x30 Å and a single-point calculation was performed in vacuo using VASP. The electronic energy of two stable gas-phase monomers was subtracted from the electronic energy of each dimer resulting in interaction energies. The most important dimers are shown in Figure 10 in the main text and their energies are presented in Table S10 below. Both in the main text figure and in the table, the symbol between square brackets indicates the symmetry operation that relates the dimer molecules, with *t* denoting translation, *g* denoting a glide plane, *i* an inversion and 2_1 a twofold screw axis. The dimer interactions between molecules related by translational symmetry propagate continuously in the crystal structure.

Table S10 Geometry of intermolecular interactions between dimers in the various polymorphs of TFA with the related dimer DFT-d energies (in kJmol^{-1}). More interactions of the same type are indicated by multiple energy values. Refer to Figure 10 in the main text for a visual representation of the dimers.

Form	**Conf**	**COOH…HOOC**	**Ph$_A$…Ph$_A$**	**Ph$_{CM}$…Ph$_{CM}$**	**Ph$_A$…Ph$_{CM}$**	**Cl…Cl^a**
I	T	$R^2_2(8)$	Stack[t] **-41.6**		T-type[t] **-13.1**, **-12.8**	Yes^b **-11.7**
II	P	$R^2_2(8)$	Stack[t] **-46.8**		Cl…Ph[g] **-14.0**, **-13.5**	-
III	P	$R^2_2(8)$	Stack[i] **-28.2**	Stack[g] **-22.9**	T-type[t'] **-21.4**, **-20.2**	-
IV”	P	$R^2_2(8)$	Stack[i] **-28.1**	Stack[i'] **-22.2**	T-type[t'] **-22.8**, **-22.3**	-
V	P	$R^2_2(8)$	Stack[i] **-28.5**	Stack[i] **-41.3**	T-type[i] **-30.9**, **-22.8**	-
VI”	P	$R^2_2(8)$	Stack[i] **-28.2**	Stack[i] **-22.2**	T-type[t] **-22.9**, **-22.3**	-
VII	P	$R^2_2(8)$	Stack[i] **-27.6**	Cl…Ph[g] **-9.4**	T-type[t] **-22.6**, **-21.3**	-
VIII	T	$R^2_2(8)$	Stack[t] **-42.3**		T-type[t] **-12.8**	Yes^c **-13.7**
IX	P	$R^2_2(8)$	T-type[2_1] **-22.2**	Stack[i] **-30.6**	T-type[t] **-19.8**, **-19.2**	-

‘ denotes a pseudo symmetry operation between symmetry independent molecules when Z’>1
“ forms IV and VI are isostructural
[a] Short Cl-Cl distance
[b] Related by glide plane
[c] Related by inversion but continuous

The analysis of these interactions can be a complementary tool in the identification of crystal forms as suggested by Gavezzotti.[17] Then, the structural similarity already discussed between TFA-III, TFA-IV and TFA-VI is once again clear by looking at the most relevant dimer interactions (their nature and energies), and the differences between these crystal forms arise solely by subtle conformational differences between TFA molecules in the asymmetric unit (TFA-III Z'=2, TFA-IV Z'=3, TFA-VI Z'=1). Moreover, as discussed in the main text, continuous intermolecular interactions can be determinant for the different kinetics of crystallisation between polymorphs.

We note that one of the inversion-related dimers in form V (CSD refcode KAXXAI04) has an energy comparable to that of the most stabilising Stack[t] dimers of forms I, II and VIII. However, while this dimer has a particularly favourable stacking geometry, the other component of the disorder results in C-H···Ph contacts of the methyl groups rather than aromatic stacking (Figure S17) and the two interactions have very different energies (-41.3 and -20.4 kJ/mol, respectively). Lopez-Mejias et al. also found this discrepancy when they calculated the lattice energies of the two disorder components for this structure (-141 and -153 kJ/mol) and they suggested that form V is unlikely to exist as an ordered structure.[18]

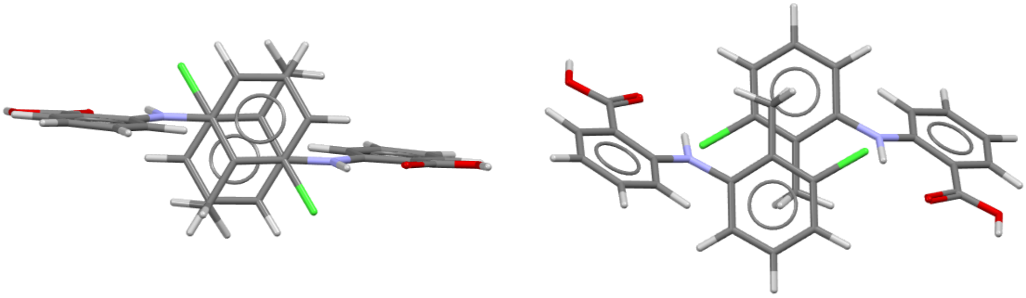

Figure S17 Geometries of the inverted stack between Ph_{CM} rings in the two disorder components of TFA-V. The geometry in component 1 (left) has an energy of -41.3 kJ/mol while component 2 (right) has a much lower energy of -20.4 kJ/mol.

Appendix – bond lengths and angles in TFA-IX

Table S1A bond lengths in TFA-IX

Atom	Atom	Length/Å		Atom	Atom	Length/Å
Cl1	C12	1.743(2)		C5	C6	1.370(3)
O1	C1	1.314(3)		C6	C7	1.402(3)
N1	C7	1.373(3)		C8	C9	1.384(3)
N1	C8	1.420(3)		C8	C13	1.400(3)
C1	O2	1.236(3)		C9	C10	1.380(3)
C1	C2	1.458(3)		C10	C11	1.370(3)
C2	C3	1.405(3)		C11	C12	1.374(3)
C2	C7	1.426(3)		C12	C13	1.397(3)
C3	C4	1.371(3)		C13	C14	1.502(3)
C4	C5	1.382(4)				

Table S2A bond angles in TFA-IX

Atom	Atom	Atom	Angle/°		Atom	Atom	Atom	Angle/°
C7	N1	C8	127.1(2)		C6	C7	C2	117.7(2)
O1	C1	C2	114.8(2)		C9	C8	N1	121.0(2)
O2	C1	O1	120.9(2)		C9	C8	C13	120.6(2)
O2	C1	C2	124.2(2)		C13	C8	N1	118.3(2)
C3	C2	C1	119.1(2)		C10	C9	C8	120.5(2)
C3	C2	C7	118.7(2)		C11	C10	C9	120.2(2)
C7	C2	C1	122.2(2)		C10	C11	C12	119.1(2)
C4	C3	C2	122.1(2)		C11	C12	Cl1	117.62(18)
C3	C4	C5	118.8(2)		C11	C12	C13	122.9(2)
C6	C5	C4	121.2(2)		C13	C12	Cl1	119.46(18)
C5	C6	C7	121.5(2)		C8	C13	C14	121.8(2)
N1	C7	C2	120.6(2)		C12	C13	C8	116.6(2)
N1	C7	C6	121.7(2)		C12	C13	C14	121.6(2)

Additional acknowledgements

PS thanks Caroline Offiler and Jordan Gaskell from the University of Manchester for the collection of FTIR data and DSC data, respectively. Additional thanks to Xiaoxia Ou and Yumin Liu for help with the translation of the patent document.

References

(1) Sheldrick, G. M. *Acta Crystallogr. Sect. C Struct. Chem.* **2015**, *71*, 3–8.

(2) Sheldrick, G. M. *Acta Crystallographica Section A: Foundations of Crystallography*. 2008, pp 112–122.

(3) Dolomanov, O. V.; Bourhis, L. J.; Gildea, R. J.; Howard, J. A. K.; Puschmann, H. *J. Appl. Crystallogr.* **2009**, *42* (2), 339–341.

(4) Farrugia, L. J. *J. Appl. Crystallogr.* **2012**, *45* (4), 849–854.

(5) Jayatilaka, D.; Wolff, S. K.; Grimwood, D. J.; McKinnon, J. J.; Spackman, M. A. *Acta Crystallogr. Sect. A Found. Crystallogr.* **2006**, *62* (a1), s90–s90.

(6) Spackman, M. A.; Jayatilaka, D. *CrystEngComm* **2009**, *11* (1), 19–32.

(7) Sacchi, P.; Lusi, M.; Cruz-Cabeza, A. J.; Nauha, E.; Bernstein, J. *CrystEngComm* **2020**, *22* (43), 7170–7185.

(8) Case, D. H.; Srirambhatla, V. K.; Guo, R.; Watson, R. E.; Price, L. S.; Polyzois, H.; Cockcroft, J. K.; Florence, A. J.; Tocher, D. A.; Price, S. L. *Cryst. Growth Des.* **2018**, *18* (9), 5322–5331.

(9) Nyman, J.; Day, G. M. *CrystEngComm* **2015**, *17* (28), 5154–5165.

(10) Francia, N. F.; Price, L. S.; Nyman, J.; Price, S. L.; Salvalaglio, M. *Cryst. Growth Des.* **2020**, *20* (10), 6847–6862.

(11) Wittering, K. E.; Agnew, L. R.; Klapwijk, A. R.; Robertson, K.; Cousen, A. J. P.; Cruickshank, D. L.; Wilson, C. C. *CrystEngComm* **2015**, *17* (19), 3610–3618.

(12) Mattei, A.; Li, T. *Pharm. Res.* **2012**, *29* (2), 460–470.

(13) Du, W.; Cruz-Cabeza, A. J.; Woutersen, S.; Davey, R. J.; Yin, Q. *Chem. Sci.* **2015**, *6* (6), 3515–3524.

(14) Penggao, C.; Du, W.; Tang, N.; Wang, D.; Xiang, J.; Jianping, Z.; Lei, Z. Tolfenamic acid new crystal form and preparation method thereof. CN107814733A, 2018.

(15) Gavezzotti, A.; Filippini, G. *J. Phys. Chem.* **1994**, *98* (18), 4831–4837.

(16) Gavezzotti, A. *Acc. Chem. Res.* **1994**, *27* (10), 309–314.

(17) Gavezzotti, A. *J. Pharm. Sci.* **2007**, *96* (9), 2232–2241.

(18) López-Mejías, V.; Kampf, J. W.; Matzger, A. J. *J. Am. Chem. Soc.* **2009**, *131* (13), 4554–4555.